Biophysical Chemistry 180–181 (2013) 135–144

Contents lists available at ScienceDirect

Biophysical Chemistry

journal homepage: http://www.elsevier.com/locate/biophyschem

Stepwise oligomerization of murine amylin and assembly of amyloid fibrils

Leonardo C. Palmieri [a,1], Bruno Melo-Ferreira [a,1], Carolina A. Braga [b,c,d,2,3], Giselle N. Fontes [e], Luana Jotha Mattos [a,1], Luís Maurício T.R. Lima [a,c,f,*,3]

[a] Laboratory for Pharmaceutical Biotechnology, School of Pharmacy, Federal University of Rio de Janeiro — UFRJ, CCS, Bss34, Ilha do Fundão, 21941-617 Rio de Janeiro, RJ, Brazil
[b] Polo Xerém, Federal University of Rio de Janeiro — UFRJ, Duque de Caxias, RJ 25245-390, Brazil
[c] Institute of Medical Biochemistry, Structural Biology Program, Federal University of Rio de Janeiro, Rio de Janeiro, RJ 21941-590, Brazil
[d] CCS, Bss42, Ilha do Fundão, Brazil
[e] Laboratory for Structural Biology (DIMAV), Brazilian National Institute of Metrology, Quality and Technology — INMETRO, Av. N. Sa. das Graças, 50 — Xerém, Duque de Caxias— 25250-020, Rio de Janeiro, Brazil
[f] National Institute of Science and Technology for Structural Biology and Bioimaging (INBEB-INCT), Federal University of Rio de Janeiro, Rio de Janeiro 21941-590, Brazil

HIGHLIGHTS

- Murine amylin spontaneously associate in low and high order oligomers.
- Murine amylin forms aggregates with amyloid fibril morphology.
- Proline-rich amylin is also capable to form amyloid structures *in vitro*.

GRAPHICAL ABSTRACT

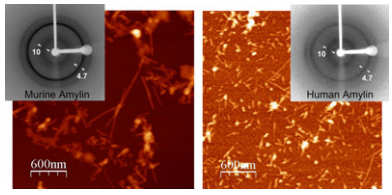

ARTICLE INFO

Article history:
Received 11 June 2013
Received in revised form 26 July 2013
Accepted 27 July 2013
Available online 6 August 2013

Keywords:
Amylin
Islet associated polypeptide
IAPP
Amyloid
Diabetes

ABSTRACT

Amylin is a pancreatic hormone co-secreted with insulin. Human amylin has been shown to form dimers and exhibit high propensity for amyloid fibril formation. We observed the ability of the water-soluble murine amylin to aggregate in water resulting in an insoluble material with Thioflavin T binding properties. Infrared spectroscopy analysis revealed beta-sheet components in the aggregated murine amylin. Morphological analysis by transmission electron microscopy and atomic force microscopy provided access to the fibril nature of the murine amylin aggregate which is similar to amyloid fibrils from human amylin. X-ray diffraction of the murine amylin fibrils showed peaks at 4.7 Å and 10 Å, a fingerprint for amyloid fibrils. Electron spray ionization–ion mobility spectroscopy–mass spectrometry (ESI-IMS-MS) analysis and crosslinking assays revealed self-association intermediates of murine amylin into high order oligomeric assemblies. These data demonstrate the stepwise association mechanism of murine amylin into stable oligomers, which ultimately converges to its organization into amyloid fibrils.

1. Introduction

Amylin (also known as islet amyloid polypeptide, IAPP) was discovered from amyloid deposit in pancreas by two independent groups [1,2]. Amyloid deposits of amylin can be found in pancreas of both diabetic and normal individuals, as well as in individuals with insulinoma [3]. The 37 amino acid peptide, amidated and with a disulfide bond between Cys2 and Cys7, is cosecreted with insulin [4] and displays several physiological functions including regulation

Abbreviations: IAPP, islet amyloid polypeptide; ESI-IMS-MS, Electrospray Ionization–Ion Mobility Spectrometry–Mass Spectrometry.

* Corresponding author at: Laboratory for Pharmaceutical Biotechnology, School of Pharmacy, Federal University of Rio de Janeiro — UFRJ, CCS, Bss34, Ilha do Fundão, 21941-617, Rio de Janeiro, RJ, Brazil. Tel./fax: +55 21 2562 6639.
E-mail address: LML@UFRJ.BR (L.M.T.R. Lima).
[1] Tel./fax: +55 21 2562 6639.
[2] Tel./fax: +55 21 26791018.
[3] Tel./fax: +55 21 2562 6761.

0301-4622/$ – see front matter © 2013 Elsevier B.V. All rights reserved.
http://dx.doi.org/10.1016/j.bpc.2013.07.013

of food intake, satiety, gastric emptying, regulation of glucose and lactate homeostasis, among others [5–8].

Human amylin displays restricted solubility in aqueous milieu, in the nanomolar concentration range [9]. Human and murine amylin are very similar, differing only in four amino acids, His^{18} and $Pro^{25,28,29}$. Proline-rich amylin variants display enhanced aqueous solubility [10]. It has been suggested that proline-rich variants of amylin in the segment comprising residues 20–29 are not prone to aggregation, and this feature would correlate with the propensity for amyloid deposition *in vivo* in mammalians [10,11]. However, metabolic disturbance in beta cells could also exert important roles in the formation of amyloid deposits containing non-proline-rich amylin [12].

These features have inspired the strategy behind the development of amylin derivatives [13,14] and amylinomimetic compounds, such as the triple mutant $Pro^{25,28,29}$ amylin analog named pramlintide, available since 2005 in the therapeutic practice for mimicking the post-prandial amylin levels in diabetic individuals [15,16]. Despite the enhanced solubility of the proline-rich variants, evidences have been found elsewhere that such human amylin analog peptides are prone to assembly into amyloid fibrils. Segments 8–20 and 14–20 of human amylin are able to form amyloid fibrils [17,18]. Also, it has been found that the equivalent segment of murine amylin spanning amino acids 8–20 (differing from human amylin solely by the His^{18}) also forms amyloid fibrils [18]. A peptide comprising the region 30–37, which share the same sequence in both human and murine amylin, also can be structured into amyloid fibrils [19]. Single-point mutation in the murine amylin sequence enhances the propensity for amyloid formation in murine amylin [20]. In fact, murine amylin has been found to form amyloid fibrils under very particular circumstances, by dissolving lyophilized amylin directly with Tris–HCl buffer pH 7.4, while attempts to dissolve with water or phosphate buffered saline did not result into amyloid fibrils [21]. Moreover, formation of murine amylin amyloid assemblies has been reported with discretion in the literature [20,22], and so far these data have not received much attention.

The collected evidences concerning amyloid fibrils formation from murine amylin fragments have been indicative that murine amylin can in fact perform homoassociation, resulting in the assembly of high order oligomers that ultimately could result in the formation of amyloid fibrils. However, the lack of experimental evidences for such intermediates and the lack of detection of amyloid deposits in rodent has been used as an excluding criteria in the assignment of murine amylin as an amyloidogenic peptide.

Amyloid assembly requires extensive conformational conversion and association of protein subunits into oligomeric assemblies which ultimately will acquire a final amyloid fibril conformation [23–28]. Indeed, evidence from distinct groups using varying methods have demonstrated the association of amylin into dimers, both murine and human amylin variants [23,29–36]. However, higher order association species have not been described, which has limited the description of a pathway for amyloid formation.

In this work we report the characterization of murine amylin self-association and amyloid fibril formation in the absence of molecular cofactors. In another aspect, our data elicits an equilibrium transition between a large conformational variability of amylin monomers and an ensemble of higher order oligomers. We discuss the self-association and further amyloid fibril formation as a general propensity of amylin, which might be under tight control of homeostasis *in vivo* which is likely to rule over the prevention of amylin amyloid aggregation.

2. Material and methods

2.1. Reagents

Murine (molecular weight 3920.045 Da; lot 129962001070611XB) and human (molecular weight 3903.33 Da; lot 81709XB) amylin (CAS 122384-88-7), carboxy-amidated and with a disulfide bond between C2 and C7 were obtained from GenScript and Genemed (murine amylin, lot 87506). The purity and identity were confirmed by electron-spray-ionization–mass-spectrometry (ESI-MS), Matrix-Assisted Laser Desorption–Time of Flight–Mass Spectrometry (MALDI-ToF-MS) analysis, SDS-PAGE and C18-reversed-phase HPLC, both by the manufacturer and the present authors (data not shown). Dry peptides were stored at −20 °C until use, and once in solution they were kept at 4 °C unless otherwise stated in the text. Type I water was obtained from distilled water by deionizing to less than 1.0 μS and filtered through a 0.22 μm pore-size membrane in a water purification system (milliQ Academic; Merck-Millipore, Brazil) immediately prior to use. All other reagents were of analytical grade. All buffers and solutions were prepared immediately prior use.

2.2. Crosslinking analysis

Crosslinking was performed by incubation of 40 μg murine amylin with 0.5% v/v glutaraldehyde for 30 min in 15 μL total volume and followed by 22.5% polyacrylamide gel electrophoresis (PAGE) containing 0.01% sodium dodecylsulfate (SDS) [37]. The gels were stained with Coomassie brilliant blue R-250 and then digitalized for further data analysis through integration using ImageJ [38]. Peak analysis was performed through a curve-fitting and integration routine using Fityk [39], assuming Gaussian functions for each peak.

2.3. Electrospray ionization–ion mobility spectrometry–mass spectrometry (ESI-IMS-MS)

ESI-IMS-MS measurements were performed in a MALDI-Synapt G1 (Waters Brazil) high definition mass spectrometer (HDMS) quadrupole-traveling wave mass spectrometer. Amylin samples were diluted to 0.5 mg/mL final concentration in 100 mM ammonium acetate buffered to pH 7.4 from 10 mg/mL stock solution, and injected at a rate of 100 nL/min, using a positive ESI with a capillary voltage of 2.8 kV and N_2g at 0.4 bar. Data were acquired over the range of *m/z* 500 to 3000 for 20 min per acquisition with repeated 3 s acquisition time per point. Mass calibration was performed on a dynamic mode with phosphoric acid. Other typical instrumental settings are as described previously [40]. Data were analyzed using DriftScope 2.1 [41] (Waters Corporation, Brazil) and MassLynx 4.1 (Waters Corporation, Brazil). Human amylin shows thus a very weak signal in the ESI-MS at aqueous buffer pH 7.4 due to a fast amyloid aggregation, as also previously reported [42], and thus a detailed ESI-IMS-MS characterization of the human amylin in similar conditions of measurements performed for murine amylin was not possible.

2.4. Atomic force microscopy (AFM)

Murine and human amylin (10 mg/mL in water) were left stand to aggregate for 1 day at 25 °C and followed by dilution to 8 μg/mL with water. From each sample 20 μL was separately applied onto freshly cleaved muscovite mica and allowed to air dry at 40% relative humidity. Samples were imaged by AFM (JPK Nanowizard III, JPK Instruments AG) operating in intermittent contact mode, using conventional silicon cantilevers (OLTESPA — Bruker Probes) at room temperature. Several images were acquired at different regions to assess the homogeneity along the surface of the samples. Images were acquired at resolution 512 × 512 pixels. AFM data analysis was performed using the software WSxM [43].

2.5. Transmission electron microscopy (TEM)

Murine and human amylin dispersed in water at 1 mg/mL were diluted to 100 μg/mL with water and placed on a carbon-coated grid for 5 min, blotted to remove excess material, and stained for 2 min with a 2% solution of uranyl acetate prepared in water. Images were digitally

collected with a Jeol 1200 electron microscope (Jeol Ltd., Tokyo, Japan) operating at 80 kV.

2.6. Attenuated total reflectance Fourier-transformed infrared spectroscopy (ATR-FTIR)

Fourier-transformed infrared spectroscopy was performed by using a total attenuated reflectance with a trapezoidal germanium crystal in a Nicolet 6700 FTIR spectrometer (Thermo Scientific, WI, USA) equipped with a liquid-nitrogen-cooled MCT (HgCdTe) detector, with 128 interferograms in a 4 cm^{-1} resolution, under a continuously purged N_{2g} atmosphere. Murine and human amylin samples were measured directly from the undissolved, solid synthetic peptide or after dispersing with water (for the formation of amyloid fibrils) for 10 mg/mL final concentration, flash-frozen with liquid nitrogen and lyophilized. Spectra were base-line corrected and normalized for the amide I, II or III bands between 1800 and 1300 cm^{-1}. 2nd derivative spectra were calculated after base-line correction, by using Norris derivative routine with segment lengths of 5 and 5 gaps between segments. All data processing was performed with Omnic 8 suite (Thermo Fisher Sci Inc., USA).

2.7. Thioflavin binding assay

Thioflavin T binding to amyloid fibrils was performed by incubation for 5 min of the preformed fibril aggregates of human or murine amylin (50 μM total protein) with ThT binding buffer (10 mM NaH_2PO_4, pH 7.4) and 70 μM ThT. Fluorescence spectra was collected in a Jasco FP-6300 spectrofluorimeter (Jasco Corporation, Brazil) by setting excitation in 440 nm and emission recorded between 460 and 600 nm at 25 °C.

2.8. X-ray diffraction

Samples of amylin fiber (10 mg/mL in water) were deposited in a silanized glass slide and allowed to air dry, and the resulting protein deposit was lifted off and subjected to X-ray diffraction at 25 °C as described previously [44] with a phi-scan of 60° in 60 s by using CuKα (1.5418 Å) radiation generated by a NOVA source installed in a SuperNova diffractometer (Agilent) operated at 40 W (50 kV and 0.8 mA), and recorded on a Titan (Agilent) CCD area detector with 1024 × 1024 pixels resolution (2 × 2 binning). The images were processed with CrysAlisPro [45].

3. Results

3.1. Thioflavin T binding to aggregated amylin

Synthetic human and murine amylin are both freely soluble in organic solvents such as TFE, HFIP and DMSO. However, human amylin shows limited solubility in aqueous milieu in the nanomolar concentration range [9]. Instead, murine amylin and other proline-rich analogs are more prone to solubilization in aqueous solution [10]. However, wild-type murine amylin has been shown to bind thioflavin T (ThT) [20,22], a known dye indicative for amyloid fibrils [46]. We have attempted to solubilize high-purity synthetic murine amylin with type I water at room temperature with gentle hand mixing and observed that a few batches from distinct manufacturers eventually did not undergo complete solubilization in water. We evaluated the thioflavin T (ThT) binding property of these samples from murine and human amylin in water. Both murine and human amylin displayed ThT-binding properties as shown by the increase in the fluorescence intensity at 480 nm compared to control, suggesting the presence of amyloid fibrils or any other organized aggregated species (Fig. 1). Differences in the total amount of ordered aggregates, binding site number, affinity, and quantum yield, intrinsically dependent on the identity of the peptide subunits, could explain differences in fluorescence intensity of ThT bound to aggregates of human or murine amylin [46].

3.2. Fourier-transformed infrared spectroscopy of aggregated murine amylin

In order to gain insight on the secondary structure content of both murine and human amylin we have performed Fourier-transformed infrared spectroscopy (FTIR) in the dry samples before and after a cycle of water suspension–aggregation–lyophilization. The amide I band comprised between 1600 and 1700 cm^{-1} is sensitive to changes in secondary structure contents in protein, in particular to beta-sheet structures characteristic of beta-sheets in amyloid fibrils, with absorption maximum at about 1620 cm^{-1} [47,48].

The original dry powder of purified peptide of human amylin, prior of any dissolution, showed a similar peak at 1660 cm^{-1} and an intense absorption peak at 1620 cm^{-1}, indicative of β-sheet structure. This profile is in consonance with the previously described human amylin amide I FTIR spectra [49]. The lack of either a maximum or a shoulder at 1673 cm^{-1} is indicative of the absence of high level of remaining TFA from synthesis [49,50] (Fig. 2). Human amylin was then dispersed in water (for 10 mg/mL final concentration) for the induction of aggregation and allowed to equilibrate for 1 day, followed by lyophilization and FTIR measurements. The water-induced aggregate exhibited FTIR spectrum similar to the original peptide assayed as provided from synthesis and purification (Fig. 2A and B).

The original dry powder of purified peptide of murine amylin, prior of any dissolution, showed a FTIR spectrum with maximum at 1660 cm^{-1}, characteristic of structures in turns (Fig. 2). No further shoulder was observed in the amide I region, as suggested by the absence of additional peaks in the 2nd derivative spectra (Fig. 2B). Upon dispersion in water (for 10 mg/mL final concentration) followed by equilibration and lyophilization, the FTIR spectra of the murine amylin revealed the appearance of an intense shoulder at about 1625 cm^{-1}, at a spectral region characteristic of β-sheet amyloid structures [19,48]. Calculating the 2nd derivative of the original spectrum allows a more detailed analysis, in which peaks and shoulders become more pronounced. In Fig. 2B we show the 2nd derivative spectra, revealing the sharp minimum at 1625 cm^{-1} in the aggregated murine amylin, indicative of the appearance of β-sheet structural elements, which is absent in the original non-aggregated murine amylin. The appearance of this β-sheet spectral contribution in the aggregated murine amylin FTIR absorption spectra suggests the formation of β-sheet elements upon hydration, not observed in the original powder of the synthetic peptide.

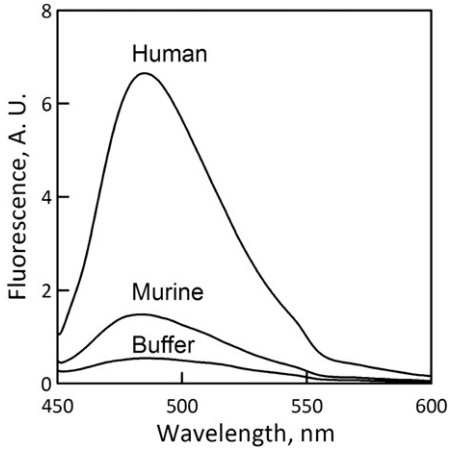

Fig. 1. Characterization of amylin aggregates by thioflavin T binding properties. Lyophilized murine and human amylin were diluted for 50 μM from a stock in water (at 10 mg/mL) in ThT binding buffer in the presence of 70 μM ThT, and allowed to incubate for 5 min at 25 °C. The ThT binding was evaluated by measuring the fluorescence emission with excitation at 440 nm. Details in the Material and methods section.

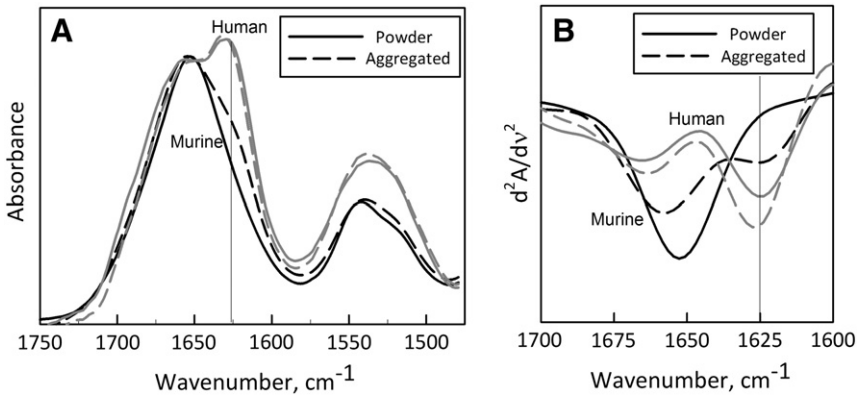

Fig. 2. FTIR measurements of murine and human amylin. Synthetic murine (black lines) and human amylin (gray lines) were dispersed with type I water for a concentration of 2.5 mM (10 mg/mL) and allowed to aggregate for 1 day at 25 °C. The samples were flash freeze with liquid nitrogen and immediately lyophilized. Dry samples were directly used for ATR-FTIR measurements, both the amylin direct from synthesis and purification (solid lines, "*Powder*") and after a cycle of water suspension and lyophilization (dashed lines, "*Aggregated*"). A) Zero order spectrum; B) 2nd derivative spectrum. Details in the Material and methods section.

3.3. Morphologic characterization of aggregated amylin by transmission electron microscopy (TEM)

We have performed transmission electron microscopy analysis of the aggregated murine and human amylin to characterize their morphology. Both samples displayed typical amyloid fibrils (Fig. 3). For human amylin we have found distinct morphologic distribution, consisting of dense amount of straight mature fibrils and thinner protofibrils (Fig. 3A and B), both similar to previously reported polymorphic nature of the human amylin fibrils [18,51,52]. No differences were observed in fibrils obtained from murine amylin incubated for 1 day (Fig. 3C and D) or 30 days (Fig. 3E and F).

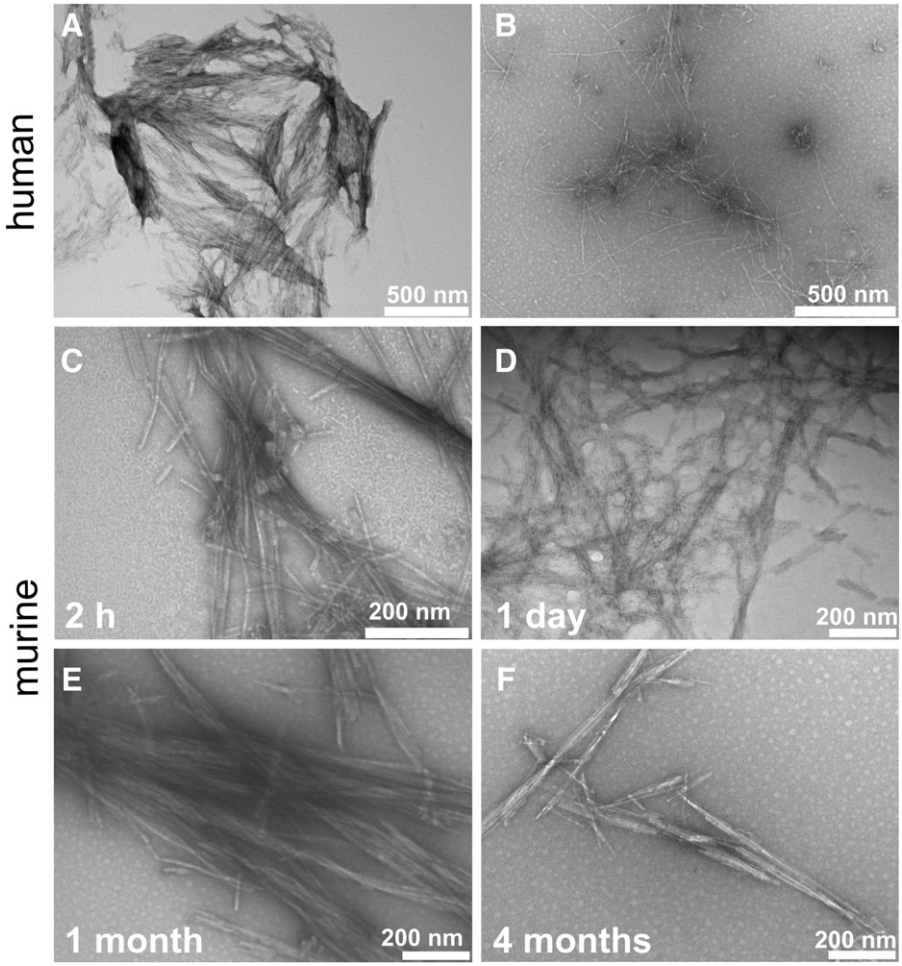

Fig. 3. TEM measurements of amyloid fibrils from murine and human amylin. Synthetic human (A and B) and murine (C, D, E and F) amylin were dissolved with type I water for a concentration of 2.5 mM (10 mg/mL) and allowed to aggregate for varying period of time: 1 day for human amylin (A and B) and 2 h (C), 1 day (D), 1 month (E) and 4 months (F) for murine amylin. At the indicated period of time, the samples were diluted and immediately prepared for TEM as described in the Material and methods section. Scale bars are depicted in their respective panels.

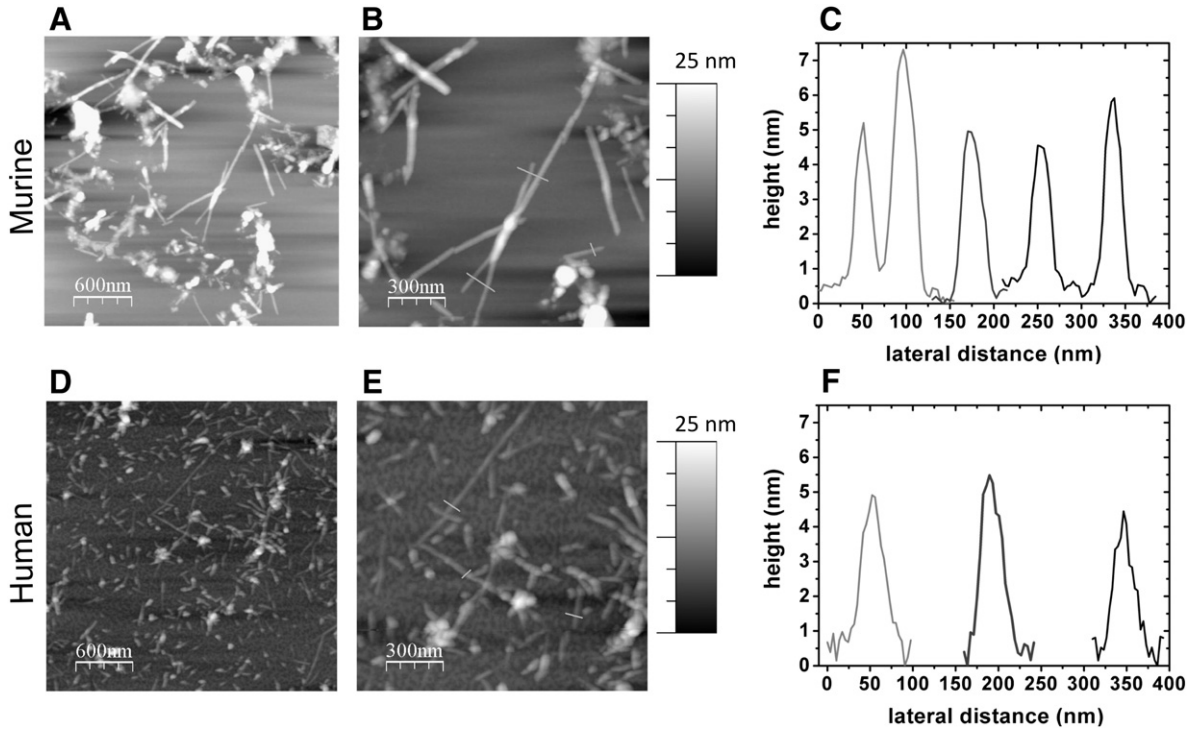

Fig. 4. AFM measurements of amyloid fibrils from murine and human amylin. Synthetic murine (A, B and C) and human (D, E and F) amylin were dissolved with type I water for a concentration of 2.5 mM (10 mg/mL) and allowed to aggregate for at least 1 day at 25 °C. The samples were diluted to a final concentration of 8 μg/mL and 20 μL were dispersed into freshly cleaved muscovite mica and allowed to dry under humidity of about 40% for 72 h before AFM measurements. (C) and (F) are height measurements of the amyloid fibrils as depicted with lines in panels (B) (murine amylin) and (E) (human amylin), respectively. The vertical scales from gray to white correspond to an overall height of 25 nm.

3.4. Atomic force microscopy analysis of amylin amyloid fibrils

Morphological analysis of the murine and human amylin was further performed by AFM, which allows direct assessment of fibril dimensions. As observed by TEM, murine amylin was showed in the AFM fibrils as long as 500 nm or longer (Fig. 4A, B), with a height of about 5 nm (Fig. 4C). The murine amylin fibrils were similar in morphology to the human amylin fibrils (Fig. 4D, E), which also showed long unbranched fibrils with heights between 4 and 6 nm (Fig. 4E and F), compatible with typical characteristics of human amylin as previously characterized by AFM and reported elsewhere [51,53].

3.5. X-ray diffraction of murine and human amyloid fibrils

Further confirmation of the amyloid nature of the aggregated murine and human amylin was performed by X-ray diffraction (XRD). Amyloid fibrils have been shown to exhibit characteristic diffraction pattern, with strong diffraction at 4.7 Å and a diffuse halo at about 10 Å, as observed from the XRD pattern of amyloid fibrils from varying proteins including amylin and amylin peptides [11,18,44,54–57].

A water suspension of each amylin fibril sample was deposited in glass slides and air dried. The nonoriented (randomly distributed) aggregated material was subjected to X-ray diffraction at room temperature by using CuKα (1.5418 Å) X-ray. A diffraction pattern was

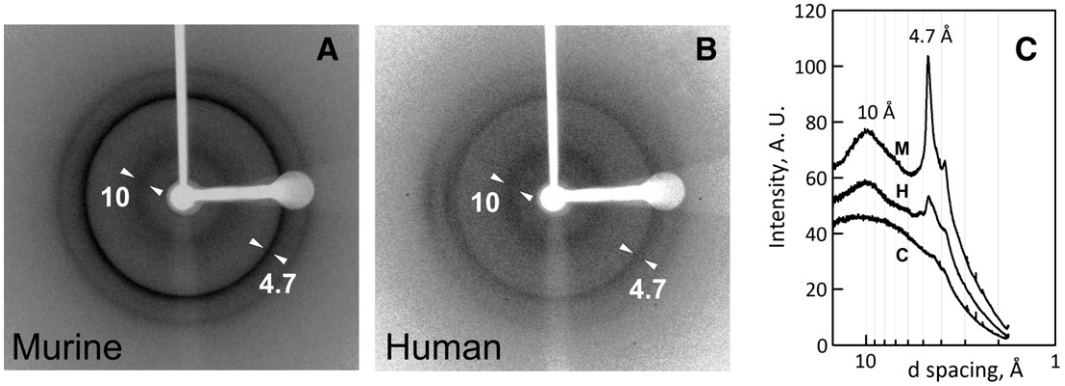

Fig. 5. X-ray diffraction pattern of nonoriented amyloid fibril from murine and human amylin. Murine (A) and human (BO amylin aggregate films were subjected to X-ray diffraction with CuKα radiation at room temperature. A and B) Diffraction image (arrow heads indicate the 4.7 Å and 10 Å diffraction rings); C) diffractogram (diffraction intensity as a function of the Bragg d-spacing) for murine (M) and human (H) amylin diffraction pattern from panels A and B respectively, and control (C) background + support. Diffuse scattering was evaluated in the absence of sample (control). Details in the Material and methods section.

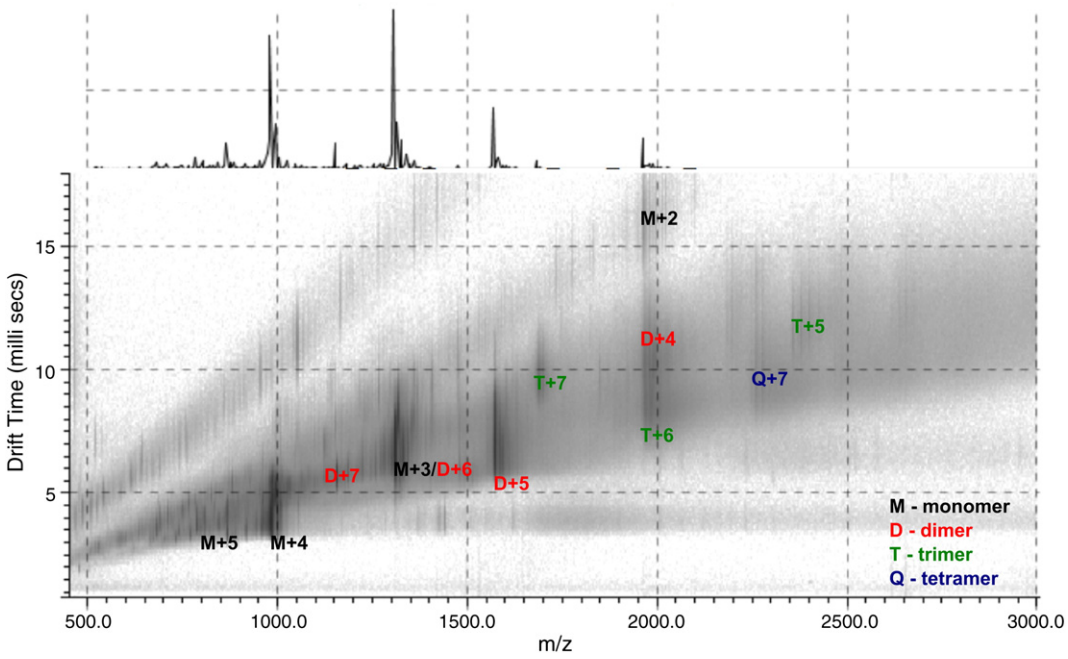

Fig. 6. Electrospray ionization/ion mobility/mass spectra of amylin. Murine amylin (10 μM in 100 mM ammonium acetate, pH 7.4) was subjected to ESI-IS-MS measurements. Letters state for the oligomeric species as depicted in legend inside the figure, and numbers following 'plus' signal are indicative of ion charge. Identification is located at the low-right side of their corresponding signals (more than one in case of multiple conformers, as depicted in Figs. 7, 8 and Table 1). Data in the 2D IMS-MS map are in log scale. At the top the total ESI-MS spectrum is shown.

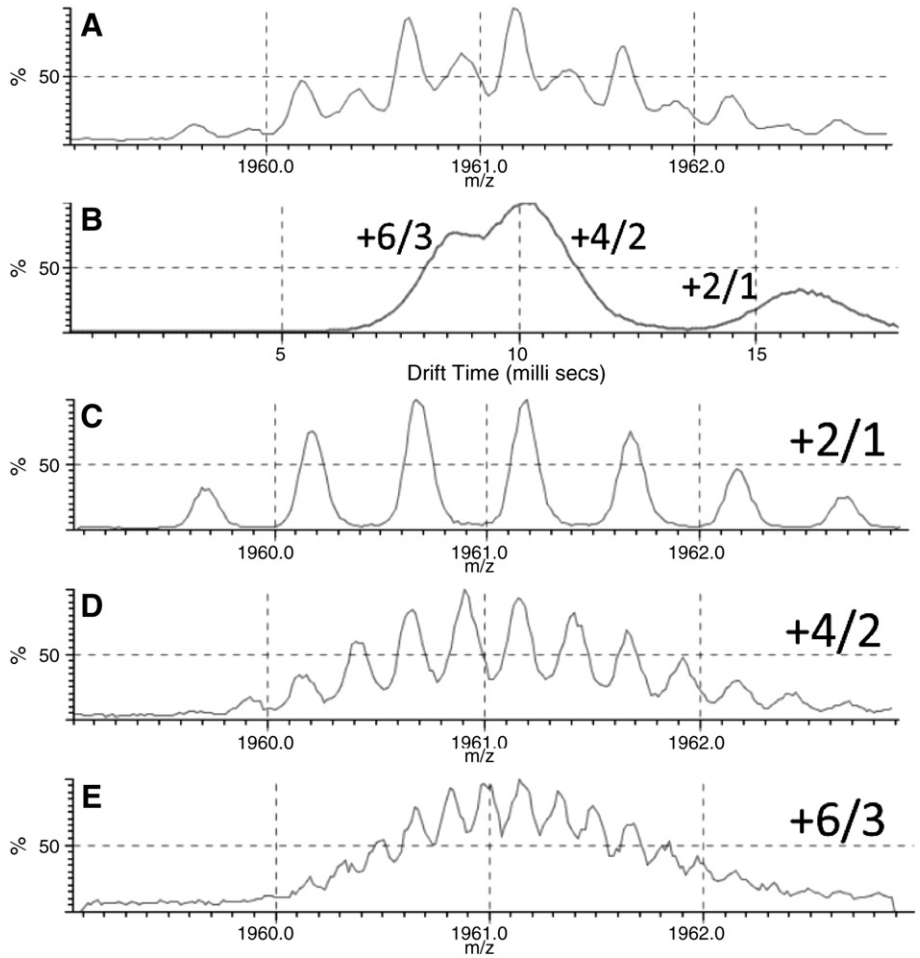

Fig. 7. Ion mobility/mass spectrometry analysis of amylin. Murine amylin was previously dissolved in DMSO at 10 mg/mL followed by dilution to 10 μM in aqueous buffer (100 mM ammonium acetate, pH 7.4) and subjected to ESI-IMS-MS measurements as described in the Material and methods section. A) Detailed view of the *m/z* 1960 ion; B) ion mobility spectra for the *m/z* 1960 ion, revealing three components at drift times 9 ms ($z/n = +6/3$), 10 ms ($z/n = +4/2$) and 16 ms ($z/n = +2/1$); C) mass spectra of the $z/n = +2/1$ ion (monomer); D) mass spectra of the $z/n = +4/2$ ion (dimer); and E) mass spectra of the $z/n = +6/3$ ion (trimer).

observed (Fig. 5), with major components at 10 Å and 4.7 Å (Fig. A and B, arrows heads), which compose a signature pattern of amyloid fibril of proteins, for both murine (Fig. 5A; C, "M") and human (Fig. 5B; C, "H") amylin.

3.6. Electrospray ionization–ion mobility spectroscopy–mass spectrometry (ESI-IMS-MS) analysis of murine amylin

Routine quality assurance analysis report from varying batches of human amylin provided by peptide manufactures typically show multiple ions by ESI-MS, including the ions of about 1560 m/z and about 1114 m/z for dimers $z/n = +5/2$ and $z/n = +7/2$, respectively, and their corresponding ions for dimers $z/n = +5/2$ and $z/n = +7/2$ for murine amylin. These data have long been indicative of the propensity for amylin dimerization.

The additional use of the ion mobility spectroscopy coupled to electrospray ionization-mass spectroscopy (ESI-IMS-MS) has also been used for further characterization of both the monomeric [34] and dimeric [36] amylin conformers. These works have contributed to intervalidate the previous evidences for a dimeric amylin species also shown by other techniques such as crystallography, molecular dynamic simulation, crosslinking and pull-down [23,29–36]. The dimeric amylin species has been attributed to be in the pathway for early oligomerization and amyloid formation of amylin. However, the subsequent steps in the assembly of amyloid fibril is still unclear [36]. The demonstration of a stepwise assembly of amylin in an organized pathway would be desirable for the description of the mechanism of amyloid fibril formation. However, the progressive amylin association into higher order molecular weight oligomers has not been previously demonstrated.

In order to gain insight in further distribution of supramolecular assemblies of amylin in aqueous solution, we have conducted high-definition electrospray ionization–ion mobility spectrometry–mass spectrometry (ESI-IMS-MS) measurements. IMS-MS allows the separation of the spectral congestion typical of ESI resulted by multiple charged species and oligomeric species, allowing the identification and accurate measurement of molecular ionic species in a polydisperse system [40,58–63].

Table 1
Distribution in the apparent number of oligomeric conformers of murine amylin. Apparent number of conformations (*) for each amylin ion as depicted from the drift time spectra in the ESI-IMS-MS analysis.

n\z	+2	+3	+4	+5	+6	+7
$[Amylin]_1$	*	**	***	**		
$[Amylin]_2$			*	**	**	**
$[Amylin]_3$				**	*	*
$[Amylin]_4$						*

Murine amylin at 10 μM in aqueous buffer (100 mM ammonium acetate, pH 7.4) was subjected to ESI-IMS-MS, revealing a complex ion distribution in the m/z space (Fig. 6). The drift space revealed three major populations for the m/z 1960 (Fig. 7A), with means 9, 10 and 16 ms (Fig. 7B), indicating that the m/z 1960 is copopulated by dissimilar amylin species. We have applied a stripping in the drift space spectra at the 1960 m/z region, revealing +2 monomer (Fig. 7C), +4 dimer (Fig. 7D) and +6 trimer (Fig. 7E).

Further analysis of the ESI-IMS-MS data allowed the characterization of three +7 ions, corresponding to dimer (Fig. 8A and B), trimer (Fig. 8C and D) and tetramer (Fig. 8E and F). The ion mobility spectra allowed the observation of two well-defined components for the z/n +7/2 ion, with drift times 6.5 ms and 7 ms (Fig. 8A), revealing thus two distinct dimer populations with charge +7.

We could detect amylin as monomer, dimers, trimers and tetramers, with charge varying from +2 to +7. Some ions such as $z/n = +7/2$ (Fig. 8A) showed two or three distributions as inferred from the distinct population in the ion mobility spectra, indicating same oligomeric order displaying distinct conformations. We have further prospected the contribution of other oligomeric species for each possible m/z value, allowing establishing a perspective view of the oligomeric and ionic distribution of amylin (Table 1). We have observed a progressive reduction

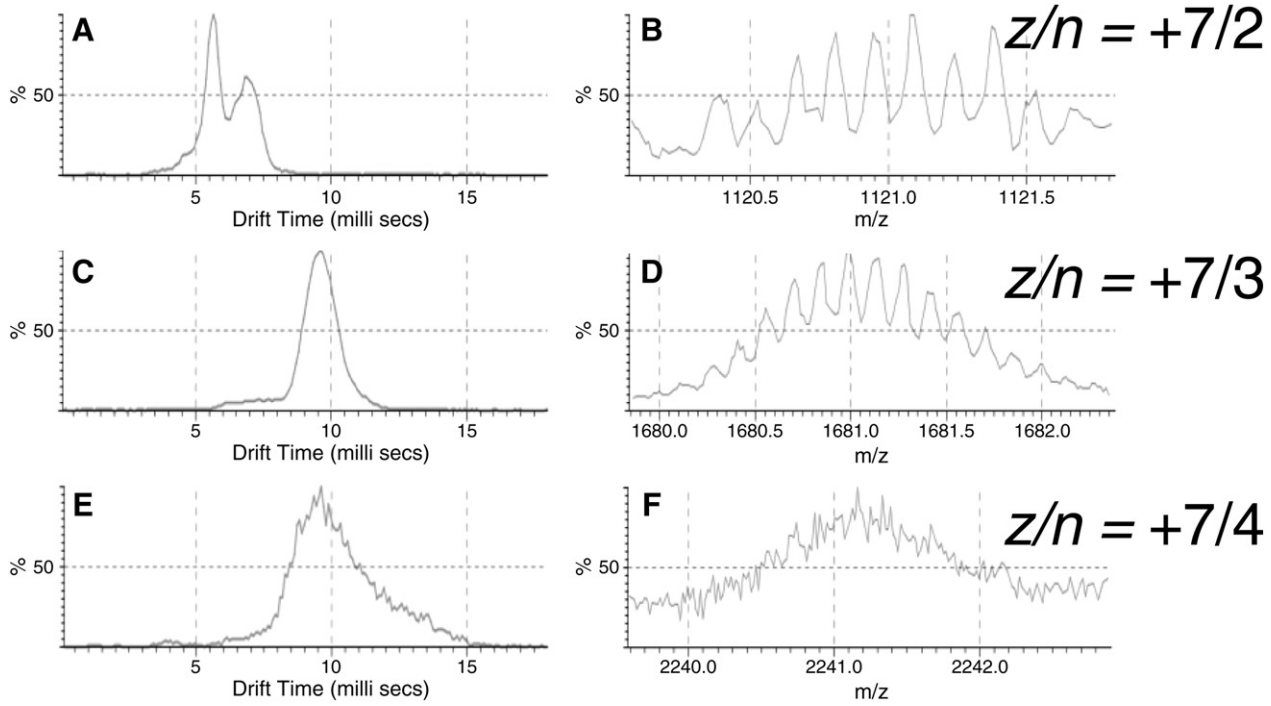

Fig. 8. Ion mobility/mass spectrometry analysis of the +7 ions of amylin. Murine amylin was previously dissolved in DMSO at 10 mg/mL followed by dilution to 10 μM in aqueous buffer (100 mM ammonium acetate, pH 7.4) and allowed to ESI-IMS-MS measurements. Ion mobility spectra (A, C and E) and mass spectra (B, D and F) of the ions $z/n = +7/2$ (dimer; A and B) $z/n = +7/3$ ion (trimer; C and D) and $z/n = +7/4$ ion (tetramer; E and F).

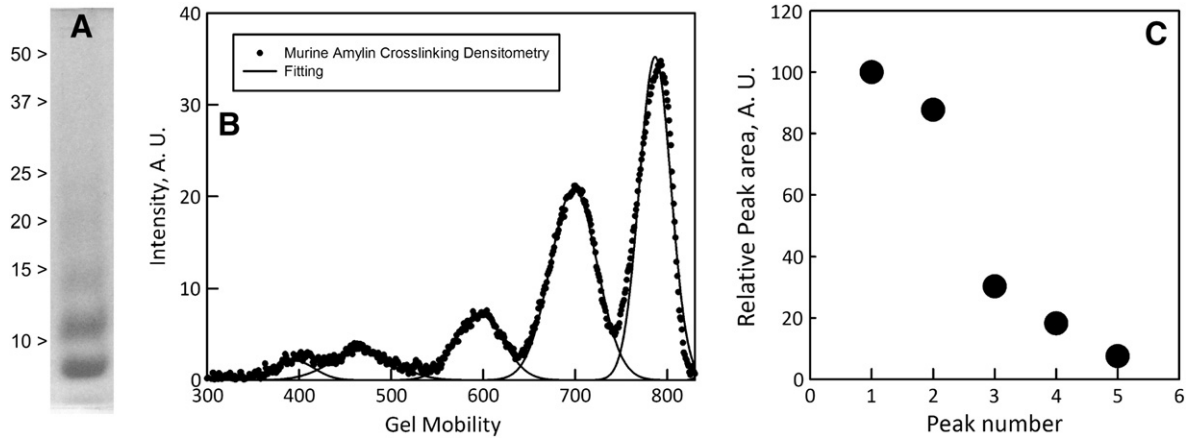

Fig. 9. Crosslinking of murine amylin. Murine amylin was crosslinked with glutaraldehyde (0.5% v/v) and the conjugation products were resolved in 22.5% SDS-PAGE. A) Digitalized gel (numbers at left side are MW in kDa from ladder run in the same SDS-PAGE); B) densitometry analysis (dots) and peak fitting (continuous lines); and C) analysis of the peak area as a function of the murine amylin crosslinking product. The details are described in the Material and methods section.

in the number of possible conformers as a function of the increasing oligomeric order, from a large distribution of monomers, with one, two and three conformers, to only one for the tetrameric amylin. A detailed estimative of the individual collision cross-section Ω could not be performed since it requires known or simulated structures with approximation for mean apparent density, and amylin displays a large conformational variability according to its milieu as evidenced by crystallography, NMR and molecular dynamic studies [31,36,64–70]. Instead, inspection of the conformational distribution of amylin oligomers indicates a steep reduction in the number of structural species as a function of the increase in the association order.

Aiming to obtain further evidences of the progressive association of murine amylin into higher order oligomers, we performed crosslinking assay in solution. A previous crosslinking study has shown the existence of a dimer of human amylin, which is related to an amyloid aggregation pathway [31]. Using similar protocol we have found at least 5 oligomers including the monomer (Fig. 9), demonstrating a stepwise association of murine amylin. This data indicate that the murine amylin is capable of performing association into dimers and higher order oligomers.

Collectively, these data suggest that amylin in solution comprises a large ensemble of conformers and oligomeric assemblies. The conformational distribution in monomeric and low order oligomeric assemblies might be a search in the conformational space for an adaptable response for each molecular partner, such as insulin, apolipoprotein E, c-peptide, proteoglycans, membrane components and zinc [71–85]. The progressive amylin self-association into species of increasing oligomeric order (Table 1) could be the preceding steps in the nucleation phase for amyloid fibril grow. We believe that these stable high order assemblies might be the result from the stepwise association of amylin monomers, progressively decreasing the conformational dispersion which culminates into a well-defined structure, which thus would pave the steps on the course of amyloid fibril formation.

4. Conclusion

The data presented here demonstrates the ability of murine amylin to associate into high order assemblies in solution, which can result in oligomers and further amyloid fibril formation. Amylin is estimated to be present in the secretory granules at high concentration range [86]. Based on the current data, we envision that amylin association and fibril formation might be a natural phenomenon that could occur in solution, in addition to the molecular conversion mediated by lipid interfaces [87]. Further proteomics and metabolomics studies may assist in the establishment of novel insights in the physiopathology of the pancreatic amyloid deposits and the onset of diabetes.

Conflict of interest

The authors confirm that this article content has no conflicts of interest.

Acknowledgments

We would like to thank Prof. Yraima Cordeiro (UFRJ) for critical reading of the manuscript, to Dr. Eduardo R. dos Santos (CEMBIO-IBCCF-UFRJ) and Dr. Daniela Lourenço (DIMAV-LaBio-INMETRO) for the excellent technical assistance with MALDI-ToF-MS and ESI-IMS-MS measurements, and to the Lab of Celular Ultrastructure Hertha Meyer (IBCCF-UFRJ) for the use of the TEM. This research was supported by Coordenação de Aperfeiçoamento de Pessoal de Nível Superior (CAPES), Nanobiotec-CAPES 04/08, Conselho Nacional de Desenvolvimento Científico e Tecnológico (CNPq), INBEB-CNPq, Fundação de Amparo à Pesquisa do Estado do Rio de Janeiro Carlos Chagas Filho (FAPERJ), LNLS and PRONEX. Funding agencies had no role in study design, data collection and analysis, decision to publish, or preparation of the manuscript.

References

[1] G.J. Cooper, A.C. Willis, A. Clark, R.C. Turner, R.B. Sim, K.B. Reid, Purification and characterization of a peptide from amyloid-rich pancreases of type 2 diabetic patients, Proceedings of the National Academy of Sciences of the United States of America 84 (1987) 8628–8632.
[2] P. Westermark, C. Wernstedt, E. Wilander, D.W. Hayden, T.D. O'Brien, K.H. Johnson, Amyloid fibrils in human insulinoma and islets of Langerhans of the diabetic cat are derived from a neuropeptide-like protein also present in normal islet cells, Proceedings of the National Academy of Sciences of the United States of America 84 (1987) 3881–3885.
[3] S.E. Kahn, S. Andrikopoulos, C.B. Verchere, Islet amyloid: a long-recognized but underappreciated pathological feature of type 2 diabetes, Diabetes 48 (1999) 241–253.
[4] A. Ogawa, V. Harris, S.K. McCorkle, R.H. Unger, K.L. Luskey, Amylin secretion from the rat pancreas and its selective loss after streptozotocin treatment, The Journal of Clinical Investigation 85 (1990) 973–976.
[5] B. Leighton, E. Foot, The effects of amylin on carbohydrate metabolism in skeletal muscle in vitro and in vivo, Biochemical Journal 269 (1990) 19–23.
[6] H.C. Fehmann, V. Weber, R. Goke, B. Goke, R. Arnold, Cosecretion of amylin and insulin from isolated rat pancreas, FEBS Letters 262 (1990) 279–281.
[7] A. Young, Amylin: Physiology and Pharmacology, Elsevier Academic Press, 2005.
[8] L. Guerreiro, D. Da Silva, D.M. Mizurini, M. Sola-Penna, L.M.T.R. Lima, Amylin induces hypoglycemia in mice, Anais da Academia Brasileira de Ciências 85 (1) (2013) 143–148, (Ref Type: Journal (Full)).
[9] G.J. Cooper, B. Leighton, G.D. Dimitriadis, M. Parry-Billings, J.M. Kowalchuk, K. Howland, J.B. Rothbard, A.C. Willis, K.B. Reid, Amylin found in amyloid deposits in human type 2 diabetes mellitus may be a hormone that regulates glycogen

metabolism in skeletal muscle, Proceedings of the National Academy of Sciences of the United States of America 85 (1988) 7763–7766.
[10] P. Westermark, U. Engstrom, K.H. Johnson, G.T. Westermark, C. Betsholtz, Islet amyloid polypeptide: pinpointing amino acid residues linked to amyloid fibril formation, Proceedings of the National Academy of Sciences of the United States of America 87 (1990) 5036–5040.
[11] G.G. Glenner, E.D. Eanes, C.A. Wiley, Amyloid fibrils formed from a segment of the pancreatic islet amyloid protein, Biochemical and Biophysical Research Communications 155 (1988) 608–614.
[12] K.H. Johnson, K. Jordan, T.D. O'Brien, M.P. Murtaugh, C. Wernstedt, C. Betsholtz, P. Westermark, Factors affecting diabetogenesis and amyloidogenesis are provided by studies of IAPP in the dog and cat, in: J.B. Natvig, O. Forre, G. Husby, A. Husebekk, B. Skogen, K. Sletten, P. Westermark (Eds.), Amyloid Amyloidosis International Symposium, Kluwer, Sweden, 1991, pp. 445–448.
[13] L.H. Guerreiro, M.F. Guterres, B. Melo-Ferreira, L.C. Erthal, R.M. da Silva, D. Lourenco, P. Tinoco, L.M. Lima, Preparation and Characterization of PEGylated Amylin, AAPS. PharmSciTech., 2013
[14] L.H. Guerreiro, S.D. Da, E. Ricci-Junior, W. Girard-Dias, C.M. Mascarenhas, M. Sola-Penna, K. Miranda, L.M. Lima, Polymeric particles for the controlled release of human amylin, Colloids and Surfaces. B, Biointerfaces 94 (2012) 101–106.
[15] A.A. Young, W. Vine, B.R. Gedulin, R. Pittner, S. Janes, L.S. Gaeta, A. Percy, C.X. Moore, J.E. Koda, T.J. Rink, K. Beaumont, Preclinical pharmacology of pramlintide in the rat: comparisons with human and rat amylin, Drug Development Research 37 (1996) 231–248.
[16] J. McQueen, Pramlintide acetate, American Journal of Health-System Pharmacy 62 (2005) 2363–2372.
[17] S. Gilead, E. Gazit, The role of the 14–20 domain of the islet amyloid polypeptide in amyloid formation, Experimental Diabetes Research 2008 (2008) 256954.
[18] E.T. Jaikaran, C.E. Higham, L.C. Serpell, J. Zurdo, M. Gross, A. Clark, P.E. Fraser, Identification of a novel human islet amyloid polypeptide beta-sheet domain and factors influencing fibrillogenesis, Journal of Molecular Biology 308 (2001) 515–525.
[19] M.R. Nilsson, D.P. Raleigh, Analysis of amylin cleavage products provides new insights into the amyloidogenic region of human amylin, Journal of Molecular Biology 294 (1999) 1375–1385.
[20] J. Green, C. Goldsbury, T. Mini, S. Sunderji, P. Frey, J. Kistler, G. Cooper, U. Aebi, Full-length rat amylin forms fibrils following substitution of single residues from human amylin, Journal of Molecular Biology 326 (2003) 1147–1156.
[21] N.G. Milton, J.R. Harris, Fibril formation and toxicity of the non-amyloidogenic rat amylin peptide, Micron 44 (2013) 246–253.
[22] PoliLopes, D.H.J., Doctoral Thesis. Title: "Peptídeo amilóide pancreático: clonagem, expressão e amiloidogênese" 2004 - Universidade Federal do Rio de Janeiro - UFRJ, Brazil.
[23] J. Cort, Z. Liu, G. Lee, S.M. Harris, K.S. Prickett, L.S. Gaeta, N.H. Andersen, Beta-structure in human amylin and two designer beta-peptides: CD and NMR spectroscopic comparisons suggest soluble beta-oligomers and the absence of significant populations of beta-strand dimers, Biochemical and Biophysical Research Communications 204 (1994) 1088–1095.
[24] A.E. Ashcroft, Mass spectrometry and the amyloid problem—how far can we go in the gas phase? Journal of the American Society for Mass Spectrometry 21 (2010) 1087–1096.
[25] B.H. Toyama, J.S. Weissman, Amyloid structure: conformational diversity and consequences, Annual Review of Biochemistry 80 (2011) 557–585.
[26] S. Bedrood, Y. Li, J.M. Isas, B.G. Hegde, U. Baxa, I.S. Haworth, R. Langen, Fibril structure of human islet amyloid polypeptide, Journal of Biological Chemistry 287 (2012) 5235–5241.
[27] L.A. Woods, G.W. Platt, A.L. Hellewell, E.W. Hewitt, S.W. Homans, A.E. Ashcroft, S.E. Radford, Ligand binding to distinct states diverts aggregation of an amyloid-forming protein, Nature Chemical Biology 7 (2011) 730–739.
[28] A.M. Ruschak, A.D. Miranker, Fiber-dependent amyloid formation as catalysis of an existing reaction pathway, Proceedings of the National Academy of Sciences of the United States of America 104 (2007) 12341–12346.
[29] A. Nath, A.D. Miranker, E. Rhoades, A membrane-bound antiparallel dimer of rat islet amyloid polypeptide, Angewandte Chemie (International Ed. in English) 50 (2011) 10859–10862.
[30] Y. Mazor, S. Gilead, I. Benhar, E. Gazit, Identification and characterization of a novel molecular-recognition and self-assembly domain within the islet amyloid polypeptide, Journal of Molecular Biology 322 (2002) 1013–1024.
[31] J.J. Wiltzius, S.A. Sievers, M.R. Sawaya, D. Eisenberg, Atomic structures of IAPP (amylin) fusions suggest a mechanism for fibrillation and the role of insulin in the process, Protein Science 18 (2009) 1521–1530.
[32] M.R. Sawaya, S. Sambashivan, R. Nelson, M.I. Ivanova, S.A. Sievers, M.I. Apostol, M.J. Thompson, M. Balbirnie, J.J. Wiltzius, H.T. McFarlane, A.O. Madsen, C. Riekel, D. Eisenberg, Atomic structures of amyloid cross-beta spines reveal varied steric zippers, Nature 447 (2007) 453–457.
[33] J.J. Wiltzius, S.A. Sievers, M.R. Sawaya, D. Cascio, D. Popov, C. Riekel, D. Eisenberg, Atomic structure of the cross-beta spine of islet amyloid polypeptide (amylin), Protein Science 17 (2008) 1467–1474.
[34] N.F. Dupuis, C. Wu, J.E. Shea, M.T. Bowers, Human islet amyloid polypeptide monomers form ordered beta-hairpins: a possible direct amyloidogenic precursor, Journal of the American Chemical Society 131 (2009) 18283–18292.
[35] J. Madine, E. Jack, P.G. Stockley, S.E. Radford, L.C. Serpell, D.A. Middleton, Structural insights into the polymorphism of amyloid-like fibrils formed by region 20–29 of amylin revealed by solid-state NMR and X-ray fiber diffraction, Journal of the American Chemical Society 130 (2008) 14990–15001.
[36] N.F. Dupuis, C. Wu, J.E. Shea, M.T. Bowers, The amyloid formation mechanism in human IAPP: dimers have beta-strand monomer-monomer interfaces, Journal of the American Chemical Society 133 (2011) 7240–7243.
[37] U.K. Laemmli, Cleavage of structural proteins during the assembly of the head of bacteriophage T4, Nature 227 (1970) 680–685.
[38] C.A. Schneider, W.S. Rasband, K.W. Eliceiri, NIH Image to ImageJ: 25 years of image analysis, Nature Methods 9 (2012) 671–675.
[39] Wojdyr, M. Fityk, A general-purpose peak fitting program, Journal of Applied Crystallography 43 (2010) 1126–1128.
[40] L.C. Palmieri, M.P. Favero-Retto, D. Lourenco, L.M. Lima, A T(3)R(3) hexamer of the human insulin variant B28Asp, Biophysical Chemistry 173–174C (2013) 1–7.
[41] J.P. Williams, J.A. Lough, I. Campuzano, K. Richardson, P.J. Sadler, Use of ion mobility mass spectrometry and a collision cross-section algorithm to study an organometallic ruthenium anticancer complex and its adducts with a DNA oligonucleotide, Rapid Communications in Mass Spectrometry 23 (2009) 3563–3569.
[42] J.L. Larson, E. Ko, A.D. Miranker, Direct measurement of islet amyloid polypeptide fibrillogenesis by mass spectrometry, Protein Science 9 (2000) 427–431.
[43] I. Horcas, R. Fernandez, J.M. Gomez-Rodriguez, J. Colchero, J. Gomez-Herrero, A.M. Baro, WSXM: a software for scanning probe microscopy and a tool for nanotechnology, The Review of Scientific Instruments 78 (2007) 013705.
[44] M. Fandrich, C.M. Dobson, The behaviour of polyamino acids reveals an inverse side chain effect in amyloid structure formation, The EMBO Journal 21 (2002) 5682–5690.
[45] Agilent Technologies, CrysAlisPro Software system. [1.171.35.19], Agilent Technologies UK Ltd., Oxford, UK, 2011.
[46] H. LeVine III, Quantification of beta-sheet amyloid fibril structures with thioflavin T, Methods in Enzymology 309 (1999) 274–284.
[47] H. Hiramatsu, T. Kitagawa, FT-IR approaches on amyloid fibril structure, Biochimica et Biophysica Acta 1753 (2005) 100–107.
[48] G. Zandomeneghi, M.R. Krebs, M.G. McCammon, M. Fandrich, FTIR reveals structural differences between native beta-sheet proteins and amyloid fibrils, Protein Science 13 (2004) 3314–3321.
[49] D. Radovan, V. Smirnovas, R. Winter, Effect of pressure on islet amyloid polypeptide aggregation: revealing the polymorphic nature of the fibrillation process, Biochemistry 47 (2008) 6352–6360.
[50] L.E. Valenti, M.B. Paci, C.P. De Pauli, C.E. Giacomelli, Infrared study of trifluoroacetic acid unpurified synthetic peptides in aqueous solution: trifluoroacetic acid removal and band assignment, Analytical Biochemistry 410 (2011) 118–123.
[51] C.S. Goldsbury, G.J. Cooper, K.N. Goldie, S.A. Muller, E.L. Saafi, W.T. Gruijters, M.P. Misur, A. Engel, U. Aebi, J. Kistler, Polymorphic fibrillar assembly of human amylin, Journal of Structural Biology 119 (1997) 17–27.
[52] A. Abedini, D.P. Raleigh, The role of His-18 in amyloid formation by human islet amyloid polypeptide, Biochemistry 44 (2005) 16284–16291.
[53] J. Seeliger, K. Weise, N. Opitz, R. Winter, The effect of Abeta on IAPP aggregation in the presence of an isolated beta-cell membrane, Journal of Molecular Biology 421 (2012) 348–363.
[54] E.D. Eanes, G.G. Glenner, X-ray diffraction studies on amyloid filaments, Journal of Histochemistry & Cytochemistry 16 (1968) 673–677.
[55] M.F. Perutz, J.T. Finch, J. Berriman, A. Lesk, Amyloid fibers are water-filled nanotubes, PNAS 99 (2002) 5591–5595.
[56] M. Sunde, C. Blake, The structure of amyloid fibrils by electron microscopy and X-ray diffraction, Advances in Protein Chemistry 50 (1997) 123–159.
[57] P.J. Gilchrist, J.P. Bradshaw, Amyloid formation by salmon calcitonin, Biochimica et Biophysica Acta 1182 (1993) 111–114.
[58] S.A. Berkowitz, J.R. Engen, J.R. Mazzeo, G.B. Jones, Analytical tools for characterizing biopharmaceuticals and the implications for biosimilars, Nature Reviews Drug Discovery 11 (2012) 527–540.
[59] I.A. Kaltashov, C.E. Bobst, R.R. Abzalimov, S.A. Berkowitz, D. Houde, Conformation and dynamics of biopharmaceuticals: transition of mass spectrometry-based tools from academe to industry, Journal of the American Society for Mass Spectrometry 21 (2010) 323–337.
[60] R. Salbo, M.F. Bush, H. Naver, I. Campuzano, C.V. Robinson, I. Pettersson, T.J. Jorgensen, K.F. Haselmann, Traveling-wave ion mobility mass spectrometry of protein complexes: accurate calibrated collision cross-sections of human insulin oligomers, Rapid Communications in Mass Spectrometry 26 (2012) 1181–1193.
[61] D.P. Smith, T.W. Knapman, I. Campuzano, R.W. Malham, J.T. Berryman, S.E. Radford, A.E. Ashcroft, Deciphering drift time measurements from travelling wave ion mobility spectrometry–mass spectrometry studies, European Journal of Mass Spectrometry (Chichester, England) 15 (2009) 113–130.
[62] D.P. Smith, S.E. Radford, A.E. Ashcroft, Elongated oligomers in beta2-microglobulin amyloid assembly revealed by ion mobility spectrometry–mass spectrometry, Proceedings of the National Academy of Sciences of the United States of America 107 (2010) 6794–6798.
[63] B.T. Ruotolo, K. Giles, I. Campuzano, A.M. Sandercock, R.H. Bateman, C.V. Robinson, Evidence for macromolecular protein rings in the absence of bulk water, Science 310 (2005) 1658–1661.
[64] R.P. Nanga, J.R. Brender, S. Vivekanandan, A. Ramamoorthy, Structure and membrane orientation of IAPP in its natively amidated form at physiological pH in a membrane environment, Biochimica et Biophysica Acta 1808 (10) (2011 Oct) 2337–2342, http://dx.doi.org/10.1016/j.bbamem.2011.06.012, Epub 2011 Jun 23.
[65] J.R. Brender, K. Hartman, R.P. Nanga, N. Popovych, B.R. de la Salud, S. Vivekanandan, E.N. Marsh, A. Ramamoorthy, Role of zinc in human islet amyloid polypeptide aggregation, Journal of the American Chemical Society 132 (2010) 8973–8983.
[66] J.R. Cort, Z. Liu, G.M. Lee, K.N. Huggins, S. Janes, K. Prickett, N.H. Andersen, Solution state structures of human pancreatic amylin and pramlintide, Protein Engineering, Design & Selection 22 (2009) 497–513.
[67] J.A. Williamson, A.D. Miranker, Direct detection of transient alpha-helical states in islet amyloid polypeptide, Protein Science 16 (2007) 110–117.
[68] S.M. Patil, S. Xu, S.R. Sheftic, A.T. Alexandrescu, Dynamic alpha-helix structure of micelle-bound human amylin, Journal of Biological Chemistry 284 (2009) 11982–11991.

[69] R.P. Nanga, J.R. Brender, J. Xu, K. Hartman, V. Subramanian, A. Ramamoorthy, Three-dimensional structure and orientation of rat islet amyloid polypeptide protein in a membrane environment by solution NMR spectroscopy, Journal of the American Chemical Society 131 (2009) 8252–8261.
[70] M.N. Andrews, R. Winter, Comparing the structural properties of human and rat islet amyloid polypeptide by MD computer simulations, Biophysical Chemistry 156 (2011) 43–50.
[71] S.M. Mirhashemi, M.H. Aarabi, To determine the possible roles of two essential trace elements and ascorbic acid concerning amyloidal betasheet formation in diabetes mellitus, Scientific Research and Essays 6 (26) (2011) 5507–5512.
[72] D. Sellin, L.M. Yan, A. Kapurniotu, R. Winter, Suppression of IAPP fibrillation at anionic lipid membranes via IAPP-derived amyloid inhibitors and insulin, Biophysical Chemistry 150 (2010) 73–79.
[73] S. Janciauskiene, S. Eriksson, E. Carlemalm, B. Ahren, B cell granule peptides affect human islet amyloid polypeptide (IAPP) fibril formation in vitro, Biochemical and Biophysical Research Communications 236 (1997) 580–585.
[74] E.T. Jaikaran, M.R. Nilsson, A. Clark, Pancreatic beta-cell granule peptides form heteromolecular complexes which inhibit islet amyloid polypeptide fibril formation, Biochemical Journal 377 (2004) 709–716.
[75] S. Salamekh, J.R. Brender, S.J. Hyung, R.P. Nanga, S. Vivekanandan, B.T. Ruotolo, A. Ramamoorthy, A two-site mechanism for the inhibition of IAPP amyloidogenesis by zinc, Journal of Molecular Biology 410 (2011) 294–306.
[76] S.B. Charge, E.J. de Koning, A. Clark, Effect of pH and insulin on fibrillogenesis of islet amyloid polypeptide in vitro, Biochemistry 34 (1995) 14588–14593.
[77] D.L. MacArthur, E.J. de Koning, J.S. Verbeek, J.F. Morris, A. Clark, Amyloid fibril formation is progressive and correlates with beta-cell secretion in transgenic mouse isolated islets, Diabetologia 42 (1999) 1219–1227.
[78] J.D. Knight, J.A. Williamson, A.D. Miranker, Interaction of membrane-bound islet amyloid polypeptide with soluble and crystalline insulin, Protein Science 17 (2008) 1850–1856.
[79] L. Wei, P. Jiang, W. Xu, H. Li, H. Zhang, L. Yan, M.B. Chan-Park, X.W. Liu, K. Tang, Y. Mu, K. Pervushin, The molecular basis of distinct aggregation pathways of islet amyloid polypeptide, Journal of Biological Chemistry 286 (2011) 6291–6300.
[80] L. Wei, P. Jiang, Y.H. Yau, H. Summer, S.G. Shochat, Y. Mu, K. Pervushin, Residual structure in islet amyloid polypeptide mediates its interactions with soluble insulin, Biochemistry 48 (2009) 2368–2376.
[81] J.L. Larson, A.D. Miranker, The mechanism of insulin action on islet amyloid polypeptide fiber formation, Journal of Molecular Biology 335 (2004) 221–231.
[82] Y.C. Kudva, C. Mueske, P.C. Butler, N.L. Eberhardt, A novel assay in vitro of human islet amyloid polypeptide amyloidogenesis and effects of insulin secretory vesicle peptides on amyloid formation, Biochemical Journal 331 (Pt 3) (1998) 809–813.
[83] S. Gilead, H. Wolfenson, E. Gazit, Molecular mapping of the recognition interface between the islet amyloid polypeptide and insulin, Angewandte Chemie (International Ed. in English) 45 (2006) 6476–6480.
[84] J. Vidal, C.B. Verchere, S. Andrikopoulos, F. Wang, R.L. Hull, M. Cnop, K.L. Olin, R.C. LeBoeuf, K.D. O'Brien, A. Chait, S.E. Kahn, The effect of apolipoprotein E deficiency on islet amyloid deposition in human islet amyloid polypeptide transgenic mice, Diabetologia 46 (2003) 71–79.
[85] S. Potter-Perigo, R.L. Hull, C. Tsoi, K.R. Braun, S. Andrikopoulos, J. Teague, V.C. Bruce, S.E. Kahn, T.N. Wight, Proteoglycans synthesized and secreted by pancreatic islet beta-cells bind amylin, Archives of Biochemistry and Biophysics 413 (2003) 182–190.
[86] R.L. Hull, G.T. Westermark, P. Westermark, S.E. Kahn, Islet amyloid: a critical entity in the pathogenesis of type 2 diabetes, The Journal of Clinical Endocrinology & Metabolism 89 (2004) 3629–3643.
[87] J.D. Knight, J.A. Hebda, A.D. Miranker, Conserved and cooperative assembly of membrane-bound alpha-helical states of islet amyloid polypeptide, Biochemistry 45 (2006) 9496–9508.